doi:10.1016/j.jmb.2007.11.092 J. Mol. Biol. (2008) 376, 526–540

JMB

Available online at www.sciencedirect.com

ScienceDirect

ELSEVIER

Molecular Basis for the Unique Deubiquitinating Activity of the NF-κB Inhibitor A20

Su-Chang Lin[1]†, Jee Y. Chung[1]†, Betty Lamothe[2], Kanagalaghatta Rajashankar[3], Miao Lu[1], Yu-Chih Lo[1], Amy Y. Lam[1], Bryant G. Darnay[2]* and Hao Wu[1]*

[1]*Department of Biochemistry, Weill Medical College of Cornell University, 1300 York Avenue, New York, NY 10021, USA*

[2]*Department of Experimental Therapeutics, University of Texas M.D. Anderson Cancer Center, Houston, TX 77030, USA*

[3]*NE-CAT, Advanced Photon Source, Argonne National Laboratory, Argonne, IL 60439, USA*

Received 1 November 2007; received in revised form 20 November 2007; accepted 27 November 2007
Available online 4 December 2007

Edited by I. Wilson

Nuclear factor κB (NF-κB) activation in tumor necrosis factor, interleukin-1, and Toll-like receptor pathways requires Lys63-linked nondegradative polyubiquitination. A20 is a specific feedback inhibitor of NF-κB activation in these pathways that possesses dual ubiquitin-editing functions. While the N-terminal domain of A20 is a deubiquitinating enzyme (DUB) for Lys63-linked polyubiquitinated signaling mediators such as TRAF6 and RIP, its C-terminal domain is a ubiquitin ligase (E3) for Lys48-linked degradative polyubiquitination of the same substrates. To elucidate the molecular basis for the DUB activity of A20, we determined its crystal structure and performed a series of biochemical and cell biological studies. The structure reveals the potential catalytic mechanism of A20, which may be significantly different from papain-like cysteine proteases. Ubiquitin can be docked onto a conserved A20 surface; this interaction exhibits charge complementarity and no steric clash. Surprisingly, A20 does not have specificity for Lys63-linked polyubiquitin chains. Instead, it effectively removes Lys63-linked polyubiquitin chains from TRAF6 without dissembling the chains themselves. Our studies suggest that A20 does not act as a general DUB but has the specificity for particular polyubiquitinated substrates to assure its fidelity in regulating NF-κB activation in the tumor necrosis factor, interleukin-1, and Toll-like receptor pathways.

Keywords: A20; crystal structure; deubiquitination; DUB; TRAF6

Introduction

A20 plays an important role in cellular functions by inhibiting cell activation, cytokine signaling, and Toll-like receptor pathways.[1–6] It was originally characterized as an early-response gene to tumor necrosis factor (TNF) stimulation in human endothelial cells,[7,8] and its induction is mediated by nuclear factor κB (NF-κB).[9] As an NF-κB target gene, A20 is also induced in many other cell types by a wide range of stimuli, such as viral infection, lipopolysaccharide treatment, CD40 engagement, CD30 activation, and RANKL stimulation.[10–15]

The physiological function of A20 was first revealed by the failure to regulate TNF-induced NF-κB response in A20-deficient mice.[16] A20 is also required for termination of Toll-like receptor and intracellular sensing responses to pathogens.[17–20] It is a potential therapeutic tool for the treatment of diseases where inflammatory responses are part of the pathogenic process. Mechanistically, A20 inhibits NF-κB activation at an upstream level, leading to impaired activation of the inhibitor of κb (IκB) kinase (IKK). IKK is the kinase that phosphorylates

**Corresponding authors.* E-mail addresses: bdarnay@mdanderson.org; haowu@med.cornell.edu.

† S.-C.L. and J.Y.C. contributed equally to this work.

Present address: J. Y. Chung, Division of Therapeutic Proteins, Center for Drug Evaluation and Research, Food and Drug Administration, Bethesda, MD 20892, USA.

Abbreviations used: NF-κB, nuclear factor κB; TNF, tumor necrosis factor; IκB, inhibitor of κb; IKK, IκB kinase; IL-1, interleukin-1; UCH, ubiquitin C-terminal hydrolase; UBP, ubiquitin-processing protease; OTU, ovarian tumor; MAD, multiwavelength anomalous diffraction; PDB, Protein Data Bank; Ub-AMC, Ub-7-amino-4-methylcoumarin; GST, glutathione *S*-transferase.

NF-κB-bound IκB, leading to IκB degradation and release of NF-κB for nuclear translocation and gene transcription.[21] A20 likely directly modulates the function of upstream IKK-activating signaling proteins such as TRAF6, RIP, and, possibly, NEMO.[22–25]

NF-κB activation in the TNF, interleukin-1 (IL-1), and Toll-like receptor pathways requires Lys63-linked nondegradative polyubiquitination.[26] Using biochemical purification and *in vitro* reconstitution, it was shown that TRAF6 is a specific ubiquitin ligase (E3) in Lys63-linked polyubiquitination of itself and other proteins[27–29] and that TAK1 is the immediate upstream kinase in TRAF6-mediated IKK activation in the IL-1 and Toll-like receptor pathways.[30–35] The E2 required in this ubiquitination is a dimeric complex of Ubc13 and Uev1A. TRAF6-mediated activation of TAK1 requires the TAK1-binding adapter protein TAB2 or its homologue TAB3.[36–41] In a simplified model, TRAF6-catalyzed ubiquitination of itself leads to recruitment and subsequent ubiquitination and activation of the TAB2/TAK1 complex. TAK1 in turn phosphorylates and activates IKK.[29,42] In the related TNF pathway, RIP, rather than TRAF6, becomes polyubiquitinated via the Lys63 linkage and recruits the TAB2/TAK1 complex for IKK activation.[42]

Down-regulation of NF-κB activation by A20 depends on its dual ubiquitin-editing functions.[24,43] A20 contains a deubiquitinating enzyme (DUB) domain at its N-terminal portion[44] and multiple zinc fingers at its C-terminal portion that show redundancy in the inhibition of NF-κB activation and other functions.[8,45] While the DUB domain of A20 deubiquitinates Lys63-linked polyubiquitinated TRAF6 and RIP, the A20 C-terminal zinc fingers act as ubiquitin ligase to mediate Lys48-linked polyubiquitination. In the TNF pathway, the first function down-modulates the Lys63-linked polyubiquitination of RIP1 required for NF-κB activation, and the second function leads to RIP1 degradation. Both functions cooperate to lead to inhibition of NF-κB activation to terminate receptor signaling.[17,24,43]

DUBs hydrolyze the isopeptide bonds at ubiquitin C-termini that have been linked to other ubiquitin molecules, specific protein substrates, or small molecules. The functions of these enzymes may be quite diverse and include liberation of monomeric ubiquitin molecules from polyubiquitin and or polyubiquitinated protein substrates to recycle ubiquitin, reversal of regulatory ubiquitination, and regeneration of ubiquitin from side reactions with small-molecule nucleophiles.[46,47] Most DUBs fall into three structurally distinct families of cysteine proteases: the ubiquitin C-terminal hydrolases (UCHs), the ubiquitin-processing proteases (UBPs), and the ovarian tumor (OTU) domain-containing enzymes.[46,47] The OTU superfamily comprises a group of putative cysteine proteases that are homologous to the OTU gene product of *Drosophila*.[48] A20 has been predicted to be a member of the OTU superfamily.[48] The approximately 100 identified OTU family members include proteins from eukaryotes, viruses, and pathogenic bacteria.

In vivo, the A20 N-terminal DUB domain specifically deubiquitinates Lys63-linked polyubiquitinated TRAF6 and RIP.[17,24,43] It is presumed that this is achieved via specific disassembling of Lys63-linked polyubiquitin chains. It has also been proposed that, like other DUBs, A20 may have an active site similar to papain-like cysteine proteases.[44,48] To elucidate the molecular basis for the DUB activity of A20, we determined its crystal structure and performed a series of biochemical and cell biological studies. The structure reveals the potential catalytic mechanism of A20, which may be significantly different from papain-like cysteine proteases. Ubiquitin can be docked onto a conserved A20 surface without steric clash; this interaction exhibits charge complementarity. Surprisingly, A20 does not have specificity for Lys63-linked polyubiquitin chains. Instead, A20 effectively removes Lys63-linked polyubiquitin chains from TRAF6. Our studies argue that the specificity for particular substrates assures A20 the fidelity in regulating NF-κB activation in the TNF, IL-1, and Toll-like receptor pathways, rather than acting as a general DUB.

Results

Overall structure of the A20 DUB domain

The A20 DUB domain (residues 1–370) structure was determined from a four-wavelength Se multi-wavelength anomalous diffraction (MAD) data set on a twinned crystal (Table 1, Fig. 1a). Although twinning was suspected from the beginning, the presence of noncrystallographic translational symmetry masked the detection of twinning by intensity distributions.[49] A very similar twinning case was previously observed in the crystal of superoxide dismutase from the hyperthermophilic crenarchaeon *Pyrobaculum aerophilum*.[50] Fortunately, the pseudo-crystallographic twofold operator is close to the twinning operator, resulting in an interpretable electron density map. The twinning operator was applied only in the late stage of structural refinement. The final model contains six molecules of A20 in the crystallographic asymmetric unit and is well defined in the $2F_o - F_c$ map (Fig. 1b).

The structure folds into the shape of a teakettle, with approximate dimensions of 80 Å × 40 Å × 56 Å (Fig. 1c and d). It is composed of 10 β-strands and 10 α-helices, arranged into an anterior α-helical domain (the mouth), a central β-sandwich domain (the lid), and a posterior α-helical domain (the body). The central β-sandwich lid domain has a five-stranded β-sheet (β1–β5) opposed by a three-stranded β-sheet (β6, β9, and β10). Strands β9 and β10 further extend upward to form a β-hairpin that packs against the β-hairpin formed by strands β7 and β8. The posterior body domain is formed by helices α4–α9, while the anterior mouth domain is formed by helices α1–α3 and α10. The helices are mostly from the N-terminal half, whereas the β-strands are mostly from the C-terminal half

Table 1. Crystallographic statistics

	Four-wavelength Se-MAD diffraction data used in phase determination							
	Se-MAD data in $P3_2$ space group				Se-MAD data in $P3_212$ space group			
Wavelength	0.97917 Å	0.97935 Å	0.96411 Å	0.98714 Å	0.97917 Å	0.97935 Å	0.96411 Å	0.98714 Å
Data collection								
Space group	$P3_2$	$P3_2$	$P3_2$	$P3_2$	$P3_212$	$P3_212$	$P3_212$	$P3_212$
Cell dimensions (Å)								
a	122.9	122.9	122.9	122.9	122.9	122.9	122.9	122.9
b	122.9	122.9	122.9	122.9	122.9	122.9	122.9	122.9
c	145.2	145.3	145.2	145.3	145.2	145.3	145.2	145.3
Resolution (Å)	30–2.9	30–2.9	30–2.9	30–2.9	30–2.9	30–2.9	30–2.9	30–2.9
R_{sym} (%)	7.5 (41.9)	7.6 (44.0)	7.4 (44.4)	7.0 (44.3)	8.0 (44.0)	8.1 (45.9)	7.9 (46.7)	7.6 (46.4)
$I/\sigma I$	10.1 (2.1)	10.0 (2.0)	10.1 (2.1)	10.2 (2.0)	10.1 (2.4)	10.0 (2.1)	10.1 (2.4)	10.2 (2.3)
Completeness (%)	94.6 (51.2)	94.2 (48.7)	94.6 (52.1)	94.2 (49.9)	96.3 (60.2)	96.2 (59.8)	96.4 (63.1)	96.1 (59.6)
Redundancy (%)	6.2 (3.5)	6.2 (3.4)	6.2 (3.5)	6.2 (3.4)	11.9 (5.9)	11.8 (5.5)	11.8 (5.6)	11.7 (5.5)

	Diffraction data used in structure refinement						
Constructs	Native[a] (residues 1–370)			Remote Se 0.98714 Å; (residues 1–370)			
Data collection							
Space group	$P3_2$		$P3_212$	$P3_2$	$P3_212$	$P3_221$[b]	
Cell dimensions (Å)							
a	123.6			122.9		70.8	
b	123.6			122.9		70.8	
c	143.0			145.3		145.1	
Resolution (Å)	30–2.5		30–2.5	30–2.9	30–2.9		
R_{sym} (%)	7.2 (53.3)		7.5 (57.3)	7.0 (44.3)	7.6 (46.4)		
$I/\sigma I$	12.5 (2.7)		12.5 (4.1)	10.2 (2.0)	10.2 (2.3)		
Completeness (%)	99.9 (99.7)		99.9 (99.9)	94.2 (49.9)	96.1 (59.6)		
Redundancy (%)	5.5 (3.9)		10.4 (7.7)	6.2 (3.4)	11.7 (5.5)		
Refinement							
Space group	$P3_2$ (twin law applied)	$P3_2$	$P3_212$	$P3_2$	$P3_212$	$P3_221$ (without experimental phase)	$P3_221$ (with experimental phase)
Resolution (Å)	25–2.5	25–2.5	25–2.5	25–2.9	25–2.9	25–2.94	25–2.94
Number of reflections	79,018	81,102	41,952	50,057	26,357	9228	9228
R_{work}/R_{free} (%)	20.8/25.6	26.8/29.6	38.2/44.0	25.6/32.0	37.3/44.6	30.5/42.4	34.0/39.3
Number of atoms							
Protein	17,538	17,538	8769	17,538	8769	2923	2923
Average *B*-factors (Å^2)							
Protein	69.8	68.6	64.3	95.9	73.8	104.7	107.8
RMSD							
Bond length (Å)	0.008	0.008	0.011	0.009	0.011	0.009	0.010
Bond angle (°)	1.28	1.25	1.56	1.34	1.55	1.58	1.67
Ramachandran plot (%)							
Most favored	81.9						
Additionally allowed	16.7						
Generously allowed	1.3						

The highest-resolution shell is shown in parentheses.
[a] This column contains the final refinement statistics.
[b] The subset of reflections corresponding to the small unit cell in the $P3_221$ space group was obtained by the following transformations from the large unit cell in the $P3_212$ space group: $h' = (h-k)/3$, $k' = (h+2k)/3$, and $l' = l$.

(Fig. 2). The overall fold of the structure is different from any known structures in the Protein Data Bank (PDB) database.

The active site of A20 is formed near the center of the A20 surface in the orientation shown (Fig. 1c and d), at the junction between the lid domain and the body domain. Helix α4 from the body domain harbors the catalytic Cys103, and the β4–β5 loop of the lid domain harbors the catalytic His256, both of which are important for A20 catalysis.[44] A catalytic cleft runs horizontally at the domain interface. To the right lies the somewhat concave predicted ubiquitin-binding surface (see later discussion). Most of the A20 surface is fairly featureless, except that the active-site cleft is narrowed to the right by an elevation formed by the β1–α4 loop preceding the catalytic Cys103 and the α7–α8 loop. To the left of the active site may lay the potential binding

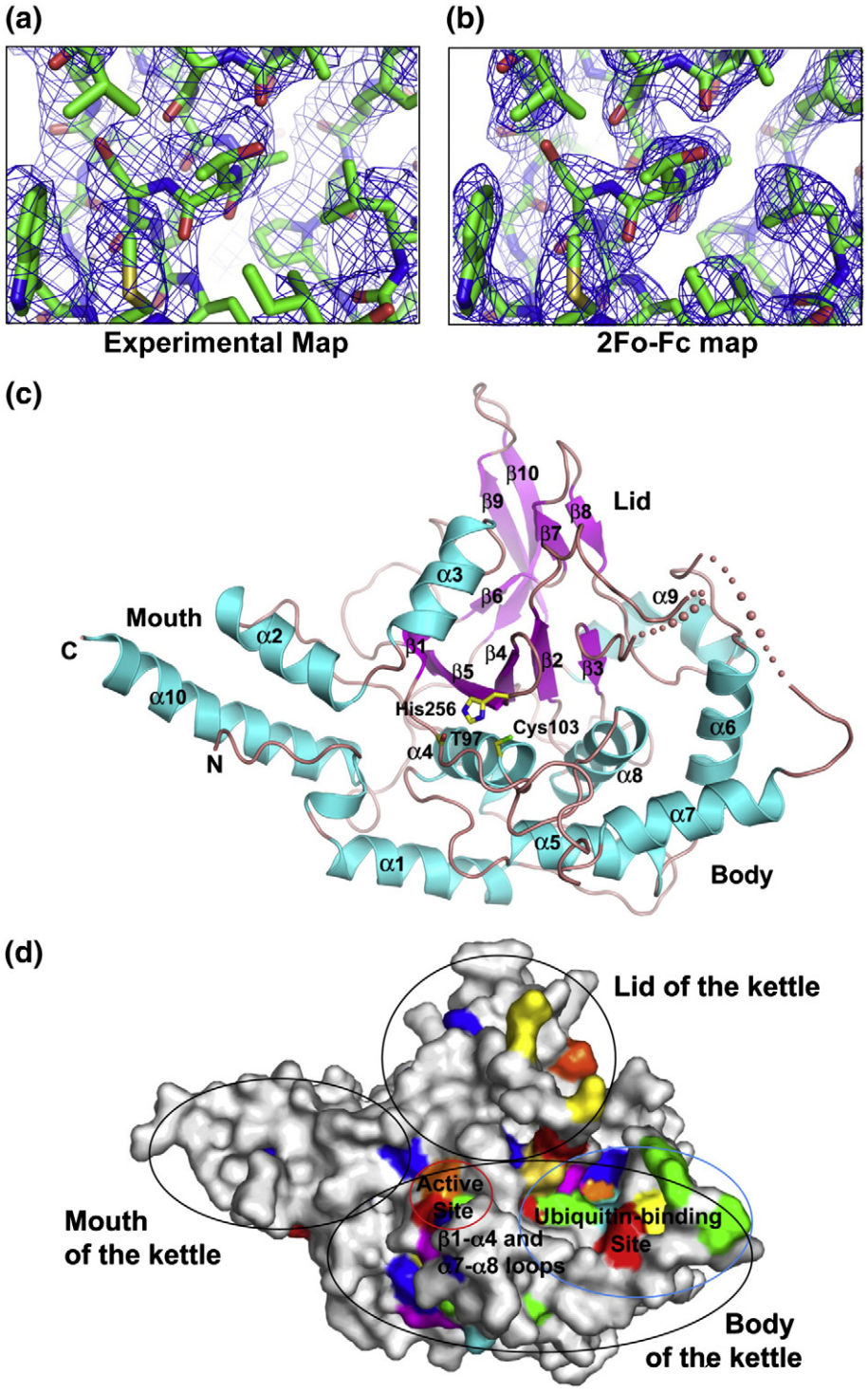

Fig. 1. Overall view of the A20 structure. (a) Experimental map from Se-MAD phasing in the small unit cell and the $P3_221$ space group. (b) The final $2F_o - F_c$ map of the same region in the $P3_2$ space group. Both maps are contoured at 1.0σ. (c) Ribbon diagram of A20. Secondary structures, active-site residues, and regions of the teakettle-shaped structure are shown. (d) Surface representation of A20 with conserved residues colored. The active site, the predicted ubiquitin-binding site, and the elevated β1–α4 and α7–α8 loops are shown.

surface for substrates such as TRAF6 and RIP1. Therefore, the surface of A20 creates an expansive platform for catalysis, ubiquitin binding, and interaction with substrates (Fig. 1d).

The mouth domain of the teakettle extends out to connect to the C-terminal domain containing multiple zinc fingers. Both the N-terminus and the C-terminus of the DUB domain reside at the mouth domain, allowing it to be inserted into other sequences. In fact, in the two A20-like proteins Cezanne and TRABID, the DUB domains are located at different regions of the sequence: one in the middle

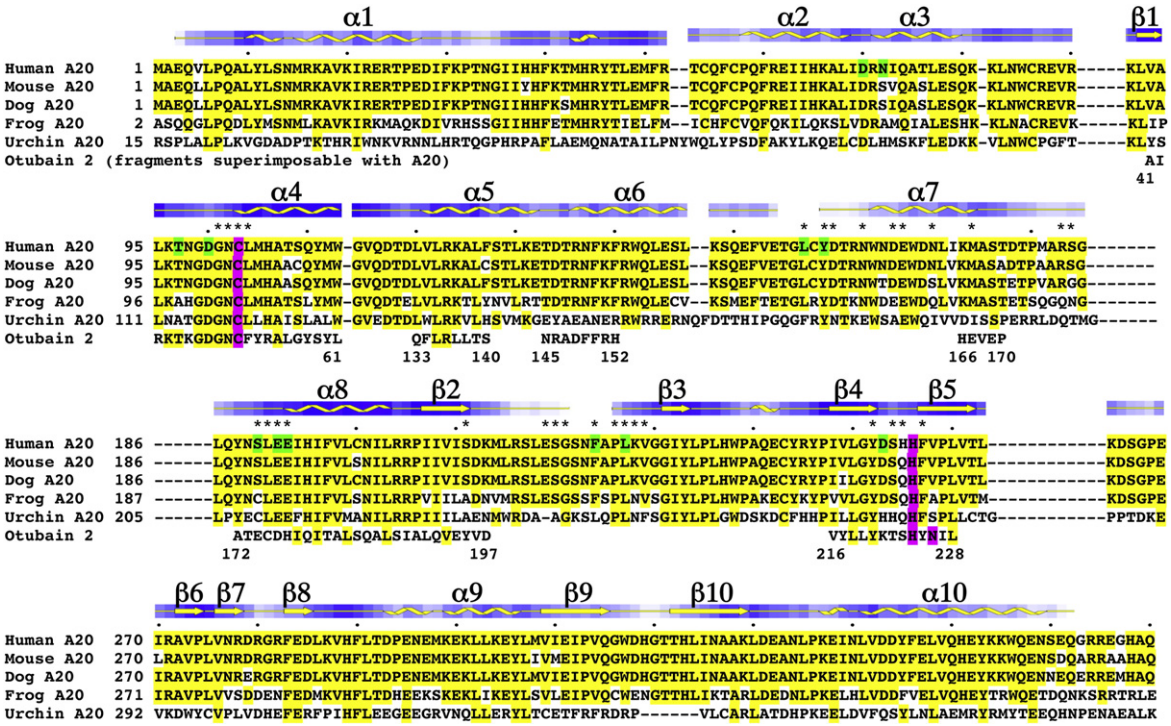

Fig. 2. Structure-based sequence alignment of A20. Every 10th residue in human A20 is indicated by a dot above the sequence. Regions of otubain 2 that are structurally aligned with A20 are also shown. Residues identical with human A20 are highlighted in yellow. Active-site residues are highlighted in magenta. Residues subjected to mutagenesis are highlighted in green. *Residues at the predicted ubiquitin-binding site.

of the protein close to the N-terminus and one near the C-terminus.[51]

Although the overall structure of the A20 DUB domain is different from those of other members of the cysteine protease superfamily such as papain, the UCHs Yuh1 and UCH-L3,[52,53] and the UBPs HAUSP, USP14, and USP2,[54–56] the arrangements of catalytic Cys and His residues are similar and conserved (Fig. 3a and b). The distance between the thiol of Cys103 and the Nδ1 atom of His256 is 3.2 Å, suggesting that the observed A20 active site is at least close to a catalytically productive conformation. This is unlike the situation in HAUSP, in which the active site exists in an unproductive conformation before ubiquitin binding.[54]

The A20 active site is most similar to that of otubain 2[57] (Fig. 3c). A structural homology search by DALI shows that 81 out of the 352 ordered residues of the A20 DUB domain can be superimposed, with an RMSD of 1.5 Å, onto the otubain 2 structure, which contains 221 residues (Figs. 2 and 3d). The superimposed regions include three β-strands (β2, β4, and β5) of the central β-sheet and four α-helices (α4, α5, α6, and α8), which contain the active site. They reside at approximately residues 100–250 of A20 and are within the predicted OTU domain. OTU is a *Drosophila* protein involved in oocyte morphogenesis.[58] Sequence signatures similar to OTU have been shown to define a new class of cysteine proteases, including A20 and otubain 2.[24,48] However, on a sequence level, A20 does not share significant homology with otubain 2. Only 19 residues are identical between A20 and otubain 2 (Fig. 2).

Potential ubiquitin-binding site

Because we were unable to obtain a complex of A20 with a ubiquitin-based suicide inhibitor such as ubiquitin aldehyde (Ubal) or Ub–Br_2 for structural studies (see later discussion), we inspected the A20 surface to see whether we could predict its ubiquitin-binding site. Strikingly, mapping of residues conserved among different species of A20 showed a highly conserved surface patch to the right of the active site (Fig. 4a). In contrast, the reverse side of A20 does not have conspicuous conserved patches (Fig. 4b). When we superimposed the A20 active site with the corresponding regions of Yuh1–Ubal (PDB ID 1XD3)[52] and HAUSP–Ubal complexes (PDB ID 1NBF),[54] the two complexes representative of the UCH and UBP families of DUBs, we found that the bound ubiquitins were both placed to the right of the active-site cleft near the conserved patch (Fig. 4c).

One important feature for the bound ubiquitins is that the locations of the C-terminal residues are very similar, although the remaining parts deviate from each other. Because the ubiquitin locations from both Yuh1 and HAUSP have some degree of steric clashes with the A20 surface, we adjusted the ubiquitin location without affecting much of the interactions at the C-terminus. Thus, an A20–ubiquitin complex with little steric clash between A20 and the bound ubiquitin can be modeled (Fig.

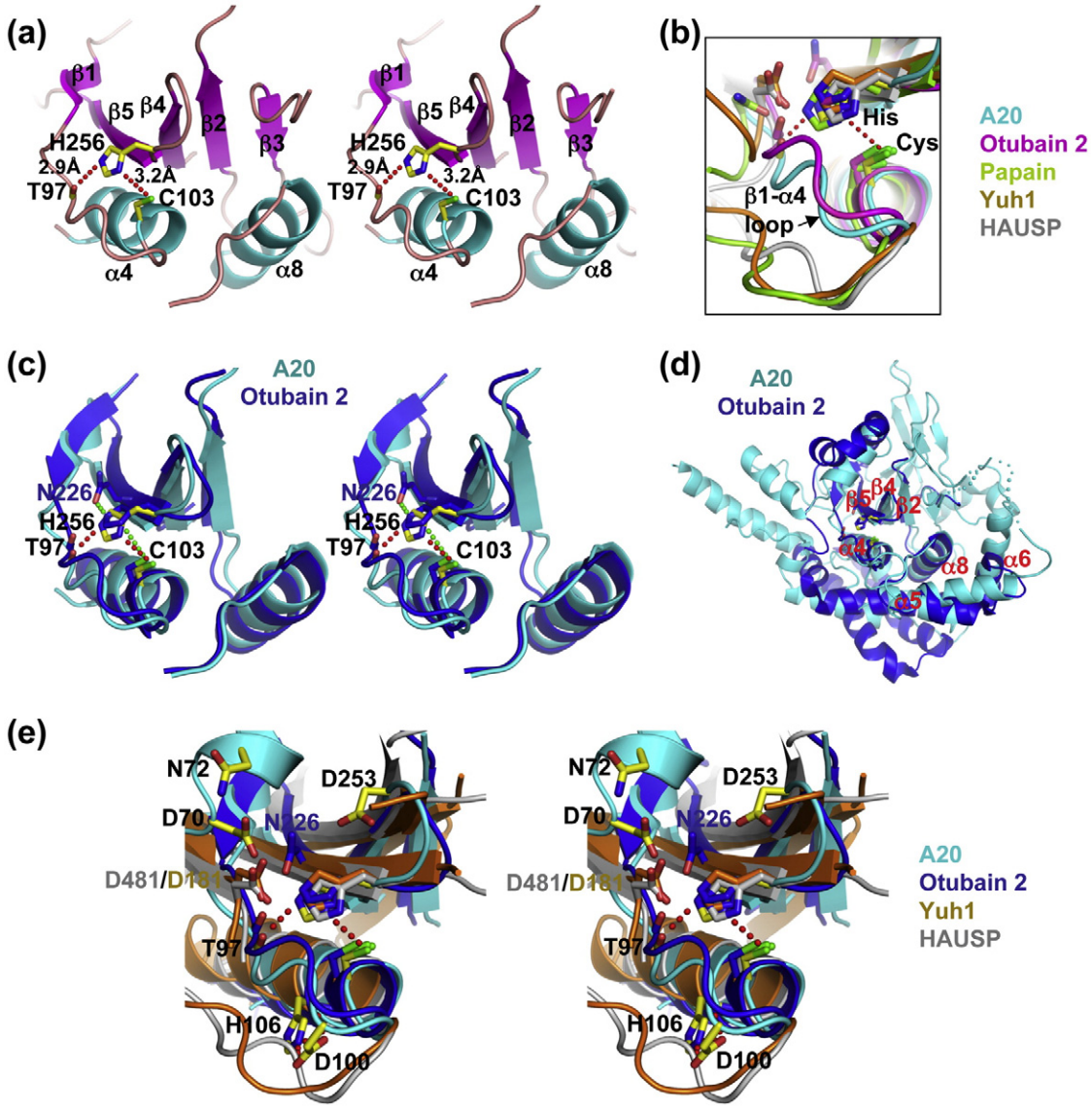

Fig. 3. The A20 active site. (a) The active site of A20 shown in stereo. The observed distances between the proposed catalytic residues Cys103, His256, and Thr97 are labeled. (b) Superposition of the A20 active site with other cysteine proteases, including papain, otubain 2, Yuh1, and HAUSP. The unusual β1–α4 loop in A20 and the corresponding loop in otubain 2 are shown. (c) Superposition of the active sites of A20 and otubain 2 in stereo. In addition to Cys103, His256, and Thr97, the proposed third catalytic residue for otubain 2, Asn226, is also shown. (d) Superposition of A20 with otubain 2, with conserved secondary structural elements labeled. (e) Superposition of the A20 active site with those of otubain 2, HAUSP, and Yuh1. Note that the third catalytic residues for otubain 2, HAUSP, and Yuh1 are Asn226, Asp481, and Asp181, respectively.

4c and d). This may also suggest that A20 likely does not undergo dramatic conformational rearrangement upon ubiquitin binding.

This modeled complex indicates that ubiquitin binding of A20 may require the surface formed by α4, α7, α8, β2, β3, β4, and β5, and the loops between them (Fig. 2). Like in other DUB–ubiquitin complexes, most of the specificity determinants appear to lie within the last five residues of ubiquitin, which assume an extended β-strand-like conformation and meander at the junction of the lid domain and the body domain. These residues are recognized extensively by A20. The two hydrophobic residues, Leu71 and Leu73 of ubiquitin, contact hydrophobic residues Pro226 and Leu227 at the disordered β2–β3 junction and Tyr252, Ser254, and His255 at β4 and the following loop (Figs. 2 and 4a). The disordered β2–β3 loop, as well as the disordered α6–α7 loop, may become ordered upon ubiquitin binding. The two positively charged residues, Arg72 and Arg74 of ubiquitin, make extensive polar and nonpolar interactions, including ion pairs with Glu192 and Glu193. Gly75 and Gly76 pass through the narrowest part of the active-site cleft, which is buttressed by the unusual β1–α4 loop and the elevated α7–α8 loop (Figs. 1c, 2, and 4a).

The modeled interaction between A20 and ubiquitin has both hydrophobic and hydrophilic com-

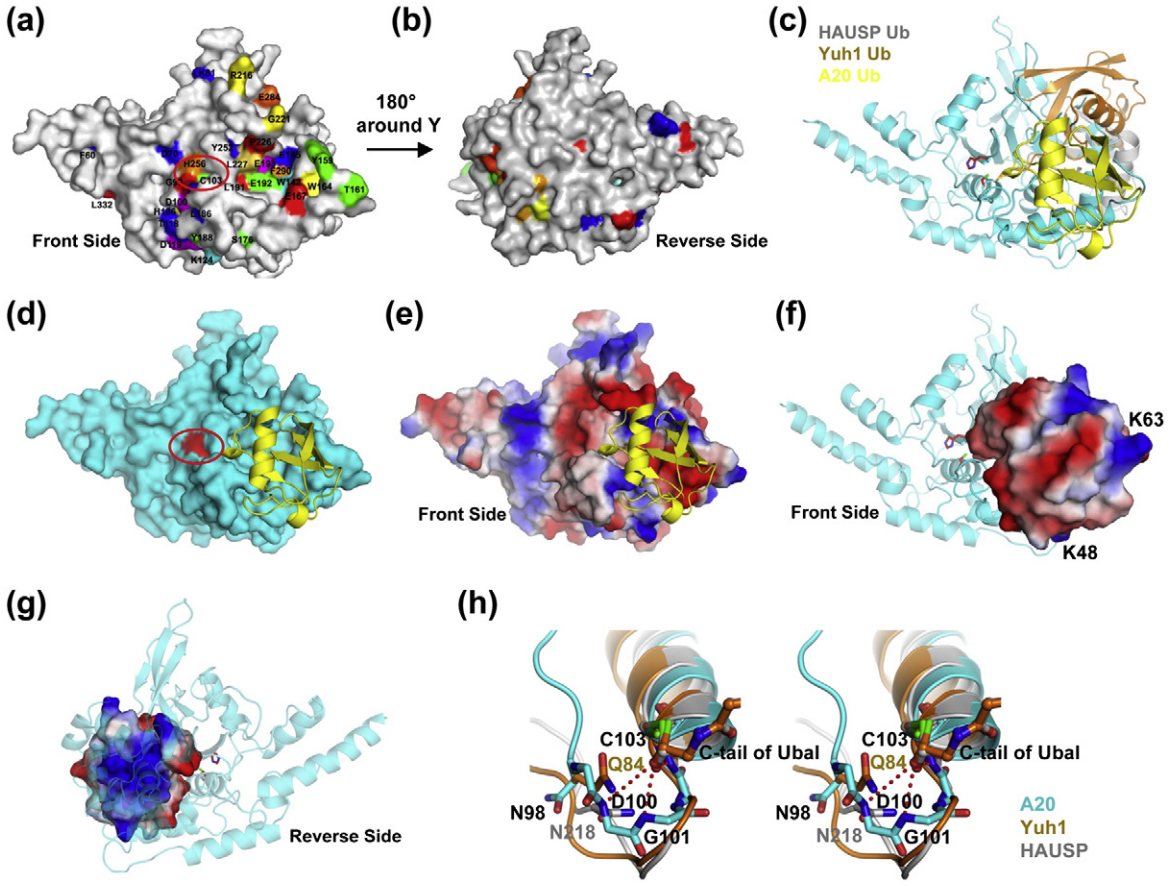

Fig. 4. The predicted interaction of A20 with ubiquitin. (a and b) Mapping of conserved residues on the A20 surface. The location of the active site is circled. (c) Ribbon diagram of A20 with modeled ubiquitins. The locations of the ubiquitin based on the HAUSP–ubiquitin and Yuh1–ubiquitin complexes are shown in gray and orange, respectively. The location of the ubiquitin after adjustment to avoid steric clash is shown in yellow. (d) Surface presentation of A20 shown in complex with the modeled ubiquitin in a ribbon diagram. The active site is circled. (e) Electrostatic surface presentation of A20 shown in complex with the modeled ubiquitin in a ribbon diagram. The ubiquitin-binding site is mostly negatively charged. (f and g) The model of the A20–ubiquitin complex shown with A20 in a ribbon diagram and the ubiquitin in an electrostatic surface representation. The positive electrostatic potential of the side of ubiquitin in contact with A20 is shown. (h) The proposed oxyanion hole construction of A20 by the main-chain amides of Cys103, Gly101, and Asp100. The corresponding regions in Yuh1 and HAUSP are superimposed and shown.

ponents (Fig. 4a and e–g). In addition, a majority of the ubiquitin-binding surface of A20 is negatively charged (Fig. 4e), complementing the positively charged surface of ubiquitin (Fig. 4g). Both Lys48 and Lys63 are exposed on the modeled bound ubiquitin, suggesting that the binding can accommodate longer ubiquitin chains (Fig. 4f). On the opposite side of the active site, the contacting region for target proteins such as TRAF6 or the upstream ubiquitin in a polyubiquitin chain may be found. This second binding site may consist of α1, α2, α3, α4, α10, and the neighboring loops.

Catalytic elements

In analogy with papain-like cysteine proteases, including DUBs with known structures, catalysis by A20 may proceed through the function of a catalytic triad. The catalytic Cys residue is thought to become deprotonated with assistance from the His residue and to attack the scissile isopeptide bond at the C-terminal Gly76 of ubiquitin. A third catalytic residue, usually an Asp or Asn, stabilizes the catalytic His. While the catalytic Cys and His residues are highly conserved between A20, otubain 2, and other cysteine proteases, the third catalytic residue of A20 is unclear. In otubain 2, the third catalytic residue is Asn226.[52,54,57] However, the corresponding residue for Asn226 of otubain 2 is Val258 of A20, making it impossible to serve this purpose. In HAUSP and Yuh1, the third catalytic residues are Asp481 and Asp181, respectively. When the active sites of A20, otubain 2, HAUSP, and Yuh1 are superimposed, Asp70 of A20 approaches the catalytic His256 from a similar direction as the known third catalytic residue, making it a possible candidate (Fig. 3e). However, the distance between the side chain of Asp70 and the Nε2 atom of His256 is 4.0 Å, which is beyond hydrogen-bonding distances.

The A20 structure shows that another candidate as a third catalytic residue, to orient the catalytic His or to stabilize the imidazolium ion, is the backbone

O atom of Thr97 at a distance of 2.9 Å (Fig. 3a and e). This residue is conserved both structurally and at the level of sequence as Thr45 in otubain 2. Although it is unusual to have a main-chain carbonyl oxygen as the third catalytic residue, there is no reason to exclude this possibility given the optimal distance of this hydrogen-bonding interaction. In addition, the side chain of Thr97 is also fairly close to His256.

Further structural analysis of A20 revealed that the side chains of residues Asp100, Asp253, and Asn72 are also within 5–10 Å of the Nε2 atom of the catalytic His256 (Fig. 3e). It has been proposed previously that Asp100 within the Cys sequence conservation region may be the third catalytic residue[48] (Fig. 2). However, the side chain of Asp100 forms hydrogen bonds with His106, helping to stabilize the loop for oxyanion hole construction (see later discussion) (Fig. 3e). Asp253 is at the tight β-hairpin between β4 and β5 that harbors the catalytic His256. It is at the center of an extensive hydrogen-bonding network with the main-chain amides of His255 and His256 and the Oγ atom of Ser254, and is therefore important for the conformation of the active site. These residues, together with Asp70 and Thr97, may be tested by mutagenesis for their roles in catalysis (see later discussion).

A comparison of the crystal structure of A20 with known DUB–ubiquitin complex structures suggests that main-chain amide atoms of Cys103, Gly101, and Asp100 may be exclusively responsible for the oxyanion hole formation in A20 (Fig. 4h). This is in contrast to the case in most cysteine proteases, in which a Gln or an Asn several residues before the active-site Cys in sequence and the backbone amide of the catalytic Cys together accommodate the negative potential formed on the carbonyl oxygen atom of the scissile bond.[52,54,59] Although there is the Asn98 residue five residues before the catalytic Cys103, its side chain points away from the putative ubiquitin scissile bond (Fig. 4h). It is possible that this is due, at least partly, to the unusual conformation of the β1–α4 loop that immediately precedes the active-site Cys103 (Fig. 3b). The loop is shifted towards Cys103 and His256, generating a much more spatially restricted active-site cleft. It likely makes it impossible for a Gln or an Asn side chain to approach the active site for oxyanion hole construction.

A20 does not have specificity for Lys63-linked polyubiquitin chains but efficiently removes Lys63-linked polyubiquitin chains from TRAF6

The first indication that A20 may be different from most DUBs came from our effort to obtain a covalent ubiquitin adduct of A20. Most DUBs are sensitive to labeling by ubiquitin-based suicide compounds such as Ubal or Ub–Br_2,[60–63] including DUBs that are specific for polyubiquitinated proteins.[54–56] However, we were only able to obtain a minute amount of the ubiquitin labeling of A20 by Ubal and a higher but still small amount of ubiquitin labeling by Ub–Br_2 (Supplementary Fig. 1). In contrast, Ubal labeled the control DUB Yuh1 efficiently (data not shown). This may be due to an extremely low activity of A20 towards single ubiquitin-based substrates. In a cleavage assay using the fluorogenic substrate Ub-7-amino-4-methylcoumarin (Ub-AMC), A20 began to show measurable activity at around 10 μM concentration, while Yuh1 at the same concentration completely cleaved all Ub-AMC substrates within a few minutes (Fig. 5a).

Although A20 has low activity towards single ubiquitin-based substrates, it does cleave polyubiquitin chains.[24,44] In fact, given that the function of A20 is in down-regulating cytokine-induced NF-κB activation through deubiquitination of Lys63-linked polyubiquitinated TRAF6, RIP, and other signaling component proteins, it is intriguing that A20 cleaves both Lys48- and Lys63-linked polyubiquitin chains. We confirmed this observation using our A20 DUB construct and Lys48- and Lys63-linked tetraubiquitin substrates (Fig. 5b). While A20 cleaved both substrates, a qualitative difference was observed. A20 disassembled Lys48-linked chains to monoubiquitin with no accumulation of diubiquitin, suggesting that Lys48-linked diubiquitin is a good substrate for A20. In contrast, both Lys63-linked diubiquitin and triubiquitin are poor substrates of A20.

To understand how A20 cleaves its substrates, we used a physiological substrate, Lys63-linked polyubiquitinated TRAF6. TRAF6 is a RING-type E3, which, in conjunction with E1 and the E2 dimeric enzyme Ubc13/Uev1A, catalyzes its autoubiquitination.[27,29] We ubiquitinated bacterially expressed glutathione *S*-transferase (GST) TRAF6 with Lys63-linked chains using the *in vitro* ubiquitination reaction. We then added A20 or its catalytic mutant C103A to determine whether A20 can deubiquitinate TRAF6. The wild-type A20 effectively deubiquitinated TRAF6 in a concentration-dependent manner (Fig. 5c). This deubiquitination manifested itself as disappearance of polyubiquitinated TRAF6. The higher-order polyubiquitinated species were more susceptible to the deubiquitination. However, we did not observe a concomitant accumulation of lower-order polyubiquitinated TRAF6, suggesting that the deubiquitination reaction did not simply transform higher-order to lower-order polyubiquitinated TRAF6 but rather removed the entire polyubiquitin chains by cleaving at the TRAF6–ubiquitin junction. As a control, the C103A mutant of A20 failed to deubiquitinate TRAF6.

Because we used Lys63-linked polyubiquitinated GST-TRAF6 and performed the deubiquitination assay in the presence of glutathione beads, we could observe the appearance of free ubiquitin chains in the supernatant of the reaction as it progressed. Surprisingly, the pattern of the polyubiquitin ladder remained the same throughout the time course (Fig. 5d), suggesting that there was negligible cleavage of the Lys63-linked polyubiquitin chains themselves. This suggests that instead of disassembling Lys63-linked polyubiquitin chains, in the presence of a specific substrate, A20 preferentially cleaves at the

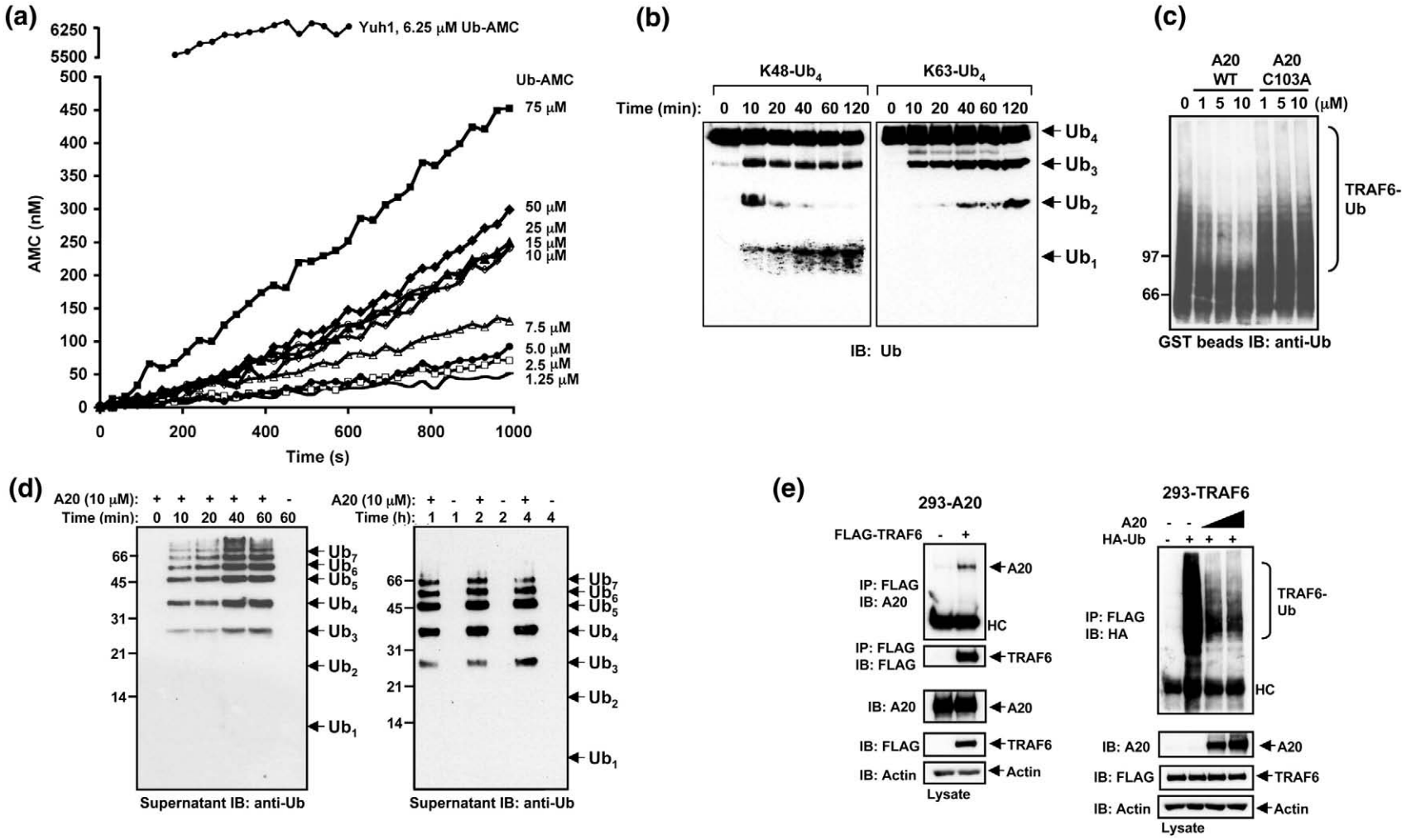

Fig. 5. A20-mediated deubiquitination. (a) Cleavage by A20 of Ub-AMC in a series of concentrations. The cleavage of Ub-AMC by the same concentration of Yuh1 is for the range between approximately 200 s and 600 s to show a complete conversion of Ub-AMC. (b) Time-dependent cleavage of Lys48-linked (left panel) and Lys63-linked (right panel) tetraubiquitin by A20. (c) Deubiquitination of Lys63-linked polyubiquitinated GST-TRAF6 by A20 at different concentrations. The active-site mutant C103A was used as a negative control. (d) A time course for deubiquitination of Lys63-linked polyubiquitinated GST-TRAF6 by A20. Deubiquitination is exemplified by the appearance of ubiquitin chains in the supernatant of glutathione beads. (e) Coimmunoprecipitation of FLAG-tagged TRAF6 and A20 (left), and deubiquitination of FLAG-tagged TRAF6 by A20 in HEK293 cells (right).

junction between the specific substrate and the polyubiquitin chain to remove its Lys63-linked polyubiquitination, leading to down-regulation of NF-κB activation. This specificity may be due to specific recognition of polyubiquitinated substrates, as shown by the interaction of A20 with TRAF6 in transfected cells (Fig. 5e). In addition, A20 transfection significantly reduced TRAF6 autopolyubiquitination (Fig. 5e).

Mutagenesis studies support an unusual catalytic mechanism and the proposed ubiquitin-binding elements

To determine whether Asp70, Asn72, Thr97, Asp100, or Asp253 may be the third catalytic residue, we mutated each to Ala (Fig. 6a–c). D70A, N72A, and T97A mutations did not have drastic effects on the ability of A20 to deubiquitinate Lys48-linked polyubiquitin or diubiquitin. These results are most surprising for D70A, as this residue situates at a location similar to the third catalytic residues in HAUSP, Yuh1, and otubain 2, and may move sufficiently close to His256 upon substrate interaction. The D100A mutation compromised A20-mediated catalysis, but this may be due to its hydrogen bonding with His106 and, therefore, its role in maintaining the conformation of the catalytic loop. The D253A mutant did not produce soluble protein, indicating that the mutation may have led to compromised A20 stability. As a control, mutation of the catalytic Cys (C103A) completely abolished A20 activity. The mutagenesis data prompted us to conclude that, unlike papain-like cysteine proteases and other DUBs, A20 most likely uses the main-chain carbonyl oxygen of Thr97 to orient the catalytic His256.

To validate our model of A20–ubiquitin interaction, we selected conserved surface residues at the putative ubiquitin-binding site. The selected residues were mutated either to Ala, such as L157A, Y159A, F224A, and L227A, or to charged residues, such as S190K and E192K, to maximize the disruption effect at the interface. The E193Q mutant has the only conservative substitution. We tested these mutants on their abilities to deubiquitinate Lys48-linked polyubiquitin chains or Lys48-linked diubiquitin (Fig. 6a and b). Both experiments showed that all mutations, except the conservative mutation of E193Q, are defective.

If these residues affect ubiquitin binding, they should also exert deleterious effects on the deubiquitination of a specific substrate, the Lys63-linked polyubiquitinated TRAF6. As predicted, with the

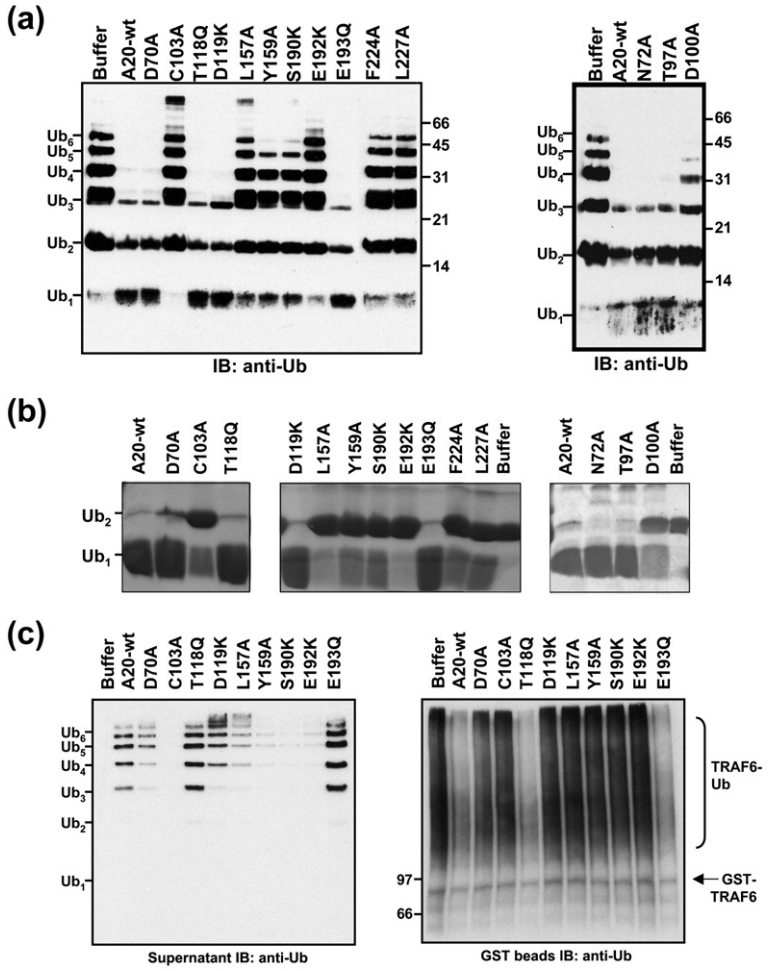

Fig. 6. Structure-based mutational analyses. (a) Cleavage of Lys48-linked polyubiquitin chains by wild-type and mutant A20. (b) Cleavage of Lys48-linked diubiquitin by wild-type and mutant A20. (c) Deubiquitination of Lys63-linked polyubiquitinated GST-TRAF6 by wild-type and mutant A20. The left panel shows the appearance of ubiquitin chains in the supernatant of glutathione beads. The right panel shows the decrease in the polyubiquitination of GST-TRAF6 bound to glutathione beads.

exception of E193Q, these mutants also abolished or reduced TRAF6 deubiquitination, in both the appearance of free polyubiquitin chains (Fig. 6c, left panel) and the ubiquitination status of GST-TRAF6 bound to glutathione beads (Fig. 6c, right panel). These data strongly support the involvement of these residues in ubiquitin binding and validate our model of the A20–ubiquitin complex.

To explore which region of A20 may be involved in TRAF6 interaction, we identified another conserved patch on the surface of A20, which is a narrow strip to the left of and below the active site (Fig. 4a). This conserved surface is not used in the modeled A20–ubiquitin complex. We recently showed that Lys124 of TRAF6 is a site of Lys63-linked TRAF6 polyubiquitination.[29] The N-terminal region of TRAF6 contains a RING finger and five zinc fingers, and Lys124 is at the junction between the RING finger and the first zinc finger. Because tandem RING and zinc fingers tend to form elongated structures, we speculated that A20 might use a long surface strip to the left side of the active site, including the identified conserved residues, to interact with TRAF6. We selected two residues for mutation in this conserved patch, T118 and D119, and generated potentially highly disruptive mutations, T118Q and D119K (Fig. 6a–c). Not surprisingly, neither mutation altered the ability of A20 to deubiquitinate Lys48-linked polyubiquitin chains (Fig. 6a and b). But surprisingly, they also did not affect the ability of A20 to deubiquitinate Lys63-linked polyubiquitinated TRAF6 (Fig. 6c). Because this patch and the predicted ubiquitin-binding surface are the only conserved surfaces of A20 (Fig. 4a and b), we speculate that the nonconserved region of the A20 surface may be important for interacting with substrates such as TRAF6 and RIP.

Discussion

There are several unexpected findings in this structural and functional analysis of A20. First, A20 does not have preferential specificity for Lys63-linked chains. Instead, it recognizes the specific polyubiquitinated substrates and cleaves at the substrate–polyubiquitin junctions. This is a surprising finding because it has been assumed based on the physiological function of A20 that it is a Lys63-specific DUB.[24,43] The surface of A20 surrounding the active site is broad and open, making it ideal for cleaving between substrates and their linked polyubiquitin chains. This is in contrast to the presence of a crossover loop directly over the active site of Yuh1, which presumably only accommodates the pass-through of small or unstructured substrates.[52] Even in comparison with otubain 2 within the same OTU superfamily, the significantly different fold and surface features around the active site would suggest that they have very different repertoires of substrates *in vivo*.

Second, A20 appears to be a "stripped-down" version of an enzyme, as many main-chain elements appear to mediate its catalysis, which differs from other DUBs and papain-like cysteine proteases in general. It is possible that the minimal active site may underlie the apparent low catalytic activity of A20. This and the specificity of A20 for particular substrates, rather than for any polyubiquitin chains, make A20 ideal for its physiological function in the reversal of regulatory ubiquitination to inhibit NF-κB signaling. Transfection of A20 does not alter the overall level of ubiquitinated cellular proteins, conjugated through either Lys63 or Lys48,[44] which is consistent with the notion that A20 does not have a global deubiquitinating activity and does not participate in ubiquitin recycling. These characteristics of A20 appear to be specific for A20 and not general for other OTU family members, as in the same study, the OTU family member Cezanne reduced the buildup of polyubiquitinated cellular proteins upon transfection.[44]

A20 is induced by NF-κB transcription, which in turn inhibits NF-κB activation by cytokines and pathogen ligands in a feedback manner. Because Lys63-linked ubiquitination has been shown to play diverse roles such as kinase activation, control of gene transcription, and DNA repair and replication,[64] it makes biological sense that A20 only deubiquitinates the specific substrates in the pathway. Both the low catalytic activity and the specificity for particular substrates of A20 assure its fidelity in this function.

While this manuscript was under preparation, Komander and Barford also reported the crystal structure of the A20 DUB domain.[65] Although the structure was solved at a lower resolution of 3.2 Å with more disordered regions, the major structural features are nonetheless very similar. However, there may be one major difference in our conclusions regarding the catalytic mechanism of the A20 DUB domain. Similar to our structural analysis, Komander and Barford also proposed that Asp70 might be the third catalytic residue, which they argue is supported by the significant effect of the D70A mutation on catalysis. Although our D70A mutation also had observable effects in some of our assays (Fig. 6b and c), the magnitude of the effects, in our assessment, does not qualify the residue as the third catalytic residue. In the classical case of serine proteases, mutations of the third catalytic residues often reduce the catalytic rates by 100-fold. One compromising scenario is that both Asp70 and the main-chain carbonyl oxygen of Thr97 participate in the orientation of His256 during catalysis, but we differ from Komander and Barford in our assessments of the relative contributions.

While the N-terminal DUB of A20 mediates deubiquitination of proteins such as TRAF6, RIP, and possibly other signaling component proteins,[17,24,25] the C-terminal zinc-finger domain of A20 mediates Lys48-linked polyubiquitination for proteasomal degradation.[24] Interestingly, for RIP and possibly for TRAF6, A20-mediated deubiquitination is a prerequisite for A20-mediated Lys48-linked polyubiquitination.[24] It is possible that only polyubiquitinated

substrates interact with A20 and, therefore, the prerequisite is due to recruitment of A20 to the NF-κB activation complex. Once recruited, A20 can mediate deubiquitination and ubiquitination using the two regions of the protein and possibly on different sites of the substrates. Although A20 has some activity in disassembling Lys48-linked polyubiquitin chains, the generally low DUB activity of A20 likely yields to its Lys48-linked polyubiquitination, leading to the degradation of the substrates. Therefore, it appears that the specificity of A20 DUB for TRAF6 and RIP controls both deubiquitination and Lys48-linked ubiquitination to inhibit NF-κB activation.

Materials and Methods

Expression, purification, and crystallization of the A20 DUB domain

To elucidate the molecular basis of A20 function, we generated a series of deletion mutants of A20 containing at least its N-terminal DUB domain. These A20 deletions were cloned into pET vectors and expressed in *Escherichia coli* by overnight IPTG induction at 20 °C. They were purified to homogeneity using Ni-affinity, ion exchange, and gel-filtration chromatography. The purified proteins were concentrated to approximately 5–10 mg/ml in 20 mM Tris (pH 7.5), 150 mM NaCl, and 10 mM DTT. As evidenced by their ability to hydrolyze polyubiquitin chains, these deletion mutants were all functional as DUBs, and the shortest deletion (residues 1–355) may represent the catalytic core domain of A20.

Three A20 constructs containing residues 1–430, 1–370, and 1–355, respectively, were crystallized using hanging drop vapor diffusion. The initial A20 crystals were derived from the construct containing residues 1–430 and diffracted poorly with strong anisotropy. Further truncations of A20 to residues 1–370 or residues 1–355 yielded crystals of a different morphology, which diffracted to 2.5 Å resolution. The crystallization condition is as follows: 1 M ammonium sulfate, 300 mM Na thiocyanate, 5 mM $MgSO_4$, and 25 mM Na cacodylate buffer at pH 6.5. Mutations of residues Q80-K81-K82 of A20 to triple Ser residues to reduce surface side-chain entropy greatly improved the reproducibility of the crystallization. Selenomethionyl substitutions were generated on one A20 construct (residues 1–370) and crystallized similarly.

Structure determination

The diffraction patterns of the A20 crystals (residues 1–370) were initially indexed and scaled in space group $P3_{1/2}12$ with cell dimensions of approximately 123 Å, 123 Å, and 146 Å, which produced indistinguishable statistics with space group $P3_{1/2}$. The crystal has noncrystallographic translational symmetry, as evidenced by strong peaks on a native Patterson map at positions (1/3, 2/3, 0) and (2/3, 1/3, 0), and contains three molecules per crystallographic asymmetric unit. By omitting weaker reflections, the diffraction data can be transformed into a smaller unit cell in space group $P3_{1/2}21$, with one-third of the original unit cell volume, cell dimensions of 71.0 Å, 71.0 Å, and 145.7 Å, and one molecule per crystallographic asymmetric unit.

The structure determination of A20 was pursued by MAD using Se as an anomalous scatterer and by multiple isomorphous replacement using Hg and other heavy atoms. More than 10 Se-MAD or Se-SAD data sets and multiple data sets from heavy-atom-soaked crystals were collected, but only the last four-wavelength Se-MAD data set at 2.9 Å resolution collected with 15° wedges for both inverse beam and different wavelengths gave the correct Se positions, determination of the hand of the space group, and a map suitable for model building. Twinning was suspected, but the diffraction data repeatedly passed twinning test.[49,66] The noncrystallographic translational symmetry may have altered the intensity statistics and masked the twinning of the crystal.[66] The structure determination was successfully performed with data indexed in the small unit cell to avoid complications from the translational symmetry.

The atomic model built from the small unit cell of the Se-Met crystal was molecularly replaced into the large unit cell of the corresponding Se-Met crystal or a native data set at 2.5 Å resolution in space group $P3_212$. Neither generated satisfactory refinement statistics and refinement was stalled. Upon the lowering of the symmetry to $P3_2$, the refinement progressed but again stalled at fairly high *R*-factors. Only by applying the correct twin law at the final refinement stage could satisfactory refinement statistics be obtained (Table 1). The final model contains six molecules of A20 in the crystallographic asymmetric unit and residues 3–362 with two disordered loops 155–158 and 222–225.

Cell lines, reagents, and antibodies

Human embryonic kidney 293 (HEK293) cells were obtained from the American Type Culture Collection (Rockville, MD) and were cultured as previously described.[29] The retroviral packaging cell line GP2-293 was purchased from Clontech (Palo Alto, CA). The following were used: monoclonal antibody to Ub (Santa Cruz Biotechnology, Santa Cruz, CA), anti-FLAG (Sigma, St. Louis, MO), rabbit polyclonal antibody to β-actin (Cytoskeleton, Denver, CO), goat anti-rabbit IgG-conjugated horseradish peroxidase (BioRad Laboratories), and goat anti-mouse IgG-conjugated horseradish peroxidase (BD Biosciences Pharmingen). Monoclonal antibody to A20 was a generous gift from Dr. S. Singh (Imgenex, San Diego, CA). Monoclonal antibody to hemagglutinin was a generous gift from Dr. G.B. Mills (University of Texas M.D. Anderson Cancer Center). Yeast E1, Ub, and poly-Ub chains (K63 and K48) were purchased from Boston Biochem (Cambridge, MA). His-tagged proteins Ubc13 and Uev1A were expressed from pET45 in *E. coli* and purified using Ni-affinity chromatography as previously described.[29]

Plasmids

Expression vectors for FLAG-TRAF6, GST-TRAF6, hemagglutinin-Ub, His-Ubc13, and His-UeV1A were used as previously described.[29] The retroviral expression vector pMX-IRES-GFP-puro (pMX-BGD) has been previously described.[29] FLAG-tagged human A20 was a generous gift from Dr. H.B. Shu (National Jewish Center, University of Colorado Health Science Center) and subsequently cloned into pMX-BGD without a FLAG tag. All site-directed mutageneses were performed using the Quik-Change kit (Stratagene) and verified by DNA sequencing.

Cleavage of Ub-AMC

A20 activity was monitored by turnover of the fluorogenic substrate Ub-AMC. Ub-AMC was purchased from Boston Biochem with a stock concentration of 2.14 mg/ml (250 μM) in 100% dimethyl sulfoxide. Fluorescence measurement upon substrate cleavage was performed on SpectraMax M2 plate reader (Molecular Devices) using 384-well plates (Corning). All measurements were performed in 20-μl reactions in 25 mM Tris (pH 8.0), 100 mM NaCl, and 5 mM DTT at 37 °C, with 10 μM A20 and various concentrations of Ub-AMC. Release of the AMC moiety was monitored at an emission wavelength of 460 nm with an excitation wavelength of 380 nm. After A20 and Ub-AMC had been added to the reaction buffer, the plate was shaken for 5 s before fluorescence reading. Reactions were monitored at 10-s intervals.

Cleavage of diubiquitin

Diubiquitin (100 μM) and A20 (5 μM) were mixed in a 10-μl reaction with 25 mM Tris buffer (pH 8.0), 5 mM DTT, and 100 mM NaCl. The mixture was incubated at 37 °C for 1 h when SDS loading buffer was added to stop the reaction. The cleavage was visualized on SDS-PAGE with Coomassie staining.

Transfection, stable HEK293 cell lines, and immunoprecipitation

Transfection of HEK293 cells was performed essentially as described.[29] Production of retroviral supernatants from GP2-293 cells transfected with pMX, pMX-FLAG-TRAF6, and pMX-A20, and infection of HEK293 cells to generate stable cells lines with the retroviral supernatants have been previously described.[29] Following transfection, the cells were harvested, lysed in buffer A for 30 min on ice, and centrifuged at 13,000 rpm for 15 min. Protein was measured on clarified lysates, and equal protein was then processed for immunoprecipitation using anti-FLAG antibody as previously described.[29]

In vitro ubiquitination of TRAF6

To generate polyubiquitinated TRAF6 for A20 DUB assays, purified GST-TRAF6 bound to glutathione agarose beads was mixed in a volume of 30 μl with the following components: 20 mM Hepes (pH 7.2), 10 mM $MgCl_2$, 25 μM MG132, 1 mM DTT, 59 μM Ub, 50 nM E1, 850 nM E2 (Ubc13/Uev1A), 1 mM ATP, 30 μM creatine phosphate, and 1 U creatine kinase. The mixture was incubated at 37 °C for 3–4 h, with gentle agitation. The beads were washed several times in buffer A (20 mM Tris pH 7.4, 250 mM NaCl, 1 mM DTT, 1 mM sodium orthovanadate, 2 mM ethylenediaminetetraacetic acid, 1% Triton X-100, 2 mg/ml leupeptin, and 2 mg/ml aprotinin), followed by three washes in low-salt buffer (20 mM Tris pH 7.4, 25 mM NaCl, and 1 mM DTT). The polyubiquitinated TRAF6 bound to beads was then used for deubiquitination assays.

Deubiquitination assays

Deubiquitination of ubiquitinated GST-TRAF6 bound to beads was performed in a final volume of 20 μl with the indicated concentration of A20 (or mutants therein) in DUB buffer (25 mM Hepes pH 7.4, 1 mM DTT, and 5 mM $MgCl_2$). Assays were conducted at 37 °C for the indicated times. After the incubation, 10 μl of cold 20 mM Hepes (pH 7.4) was added to the reaction, and samples were centrifuged for 20 min at 4 °C. A volume (20 μl) of the supernatant was collected, boiled in SDS sample buffer, subjected to SDS-PAGE, and immunoblotted with a Ub-specific antibody. The remaining GST-TRAF6 bound to the beads was then washed as described previously, followed by addition of SDS sample buffer, and then subjected to SDS-PAGE and immunoblotted with a Ub-specific antibody. Deubiquitination of free K48 or K63 polyubiquitin chains (500 ng) was performed essentially as described previously and stopped by the addition of SDS sample buffer, boiled, subjected to SDS-PAGE, and immunoblotted with a Ub-specific antibody.

Acknowledgements

We thank Igor Kourinov at The Northeastern Collaborative Access Team of Advanced Photon Source for help with diffraction data collection and Jin Wu for the maintenance of X-ray and computer equipment. This work was supported by National Institutes of Health grants (RO1 AI045937 to H.W. and RO1 AR053540 to B.G.D.) and institutional startup funds to B.G.D. S.-C.L. and Y.-C.L. are postdoctoral fellows of the Cancer Research Institute, and M.L. is a postdoctoral fellow of the American Heart Association. This work is based upon research conducted at the Northeastern Collaborative Access Team beamlines of the Advanced Photon Source, supported by award RR-15301 from the National Center for Research Resources at the National Institute of Health. Use of the Advanced Photon Source is supported by the U.S. Department of Energy, Office of Basic Energy Sciences, under Contract No. DE-AC02-06CH11357.

Supplementary Data

Supplementary data associated with this article can be found, in the online version, at doi:10.1016/j.jmb.2007.11.092

References

1. Jaattela, M., Mouritzen, H., Elling, F. & Bastholm, L. (1996). A20 zinc finger protein inhibits TNF and IL-1 signaling. *J. Immunol.* **156**, 1166–1173.
2. Cooper, J. T., Stroka, D. M., Brostjan, C., Palmetshofer, A., Bach, F. H. & Ferran, C. (1996). A20 blocks endothelial cell activation through a NF-kappaB-dependent mechanism. *J. Biol. Chem.* **271**, 18068–18073.
3. Ferran, C., Stroka, D. M., Badrichani, A. Z., Cooper, J. T. & Bach, F. H. (1997). Adenovirus-mediated gene transfer of A20 renders endothelial cells resistant to activation: a means of evaluating the role of endothelial cell activation in xenograft rejection. *Transplant. Proc.* **29**, 879–880.
4. Grey, S. T., Arvelo, M. B., Hasenkamp, W., Bach, F. H.

& Ferran, C. (1999). A20 inhibits cytokine-induced apoptosis and nuclear factor kappaB-dependent gene activation in islets. *J. Exp. Med.* **190**, 1135–1146.
5. Beyaert, R., Heyninck, K. & Van Huffel, S. (2000). A20 and A20-binding proteins as cellular inhibitors of nuclear factor-kappa B-dependent gene expression and apoptosis. *Biochem. Pharmacol.* **60**, 1143–1151.
6. O'Reilly, S. M. & Moynagh, P. N. (2003). Regulation of Toll-like receptor 4 signalling by A20 zinc finger protein. *Biochem. Biophys. Res. Commun.* **303**, 586–593.
7. Dixit, V. M., Green, S., Sarma, V., Holzman, L. B., Wolf, F. W., O'Rourke, K. *et al.* (1990). Tumor necrosis factor-alpha induction of novel gene products in human endothelial cells including a macrophage-specific chemotaxin. *J. Biol. Chem.* **265**, 2973–2978.
8. Opipari, A. W., Jr, Boguski, M. S. & Dixit, V. M. (1990). The A20 cDNA induced by tumor necrosis factor alpha encodes a novel type of zinc finger protein. *J. Biol. Chem.* **265**, 14705–14708.
9. Krikos, A., Laherty, C. D. & Dixit, V. M. (1992). Transcriptional activation of the tumor necrosis factor alpha-inducible zinc finger protein, A20, is mediated by kappa B elements. *J. Biol. Chem.* **267**, 17971–17976.
10. Laherty, C. D., Hu, H. M., Opipari, A. W., Wang, F. & Dixit, V. M. (1992). The Epstein–Barr virus LMP1 gene product induces A20 zinc finger protein expression by activating nuclear factor kappa B. *J. Biol. Chem.* **267**, 24157–24160.
11. Laherty, C. D., Perkins, N. D. & Dixit, V. M. (1993). Human T cell leukemia virus type I Tax and phorbol 12-myristate 13-acetate induce expression of the A20 zinc finger protein by distinct mechanisms involving nuclear factor kappa B. *J. Biol. Chem.* **268**, 5032–5039.
12. Tewari, M., Wolf, F. W., Seldin, M. F., Shea, O'K. S., Dixit, V. M. & Turka, L. A. (1995). Lymphoid expression and regulation of A20, an inhibitor of programmed cell death. *J. Immunol.* **154**, 1699–1706.
13. Sarma, V., Lin, Z., Clark, L., Rust, B. M., Tewari, M., Noelle, R. J. & Dixit, V. M. (1995). Activation of the B-cell surface receptor CD40 induces A20, a novel zinc finger protein that inhibits apoptosis. *J. Biol. Chem.* **270**, 12343–12346.
14. Hu, X., Yee, E., Harlan, J. M., Wong, F. & Karsan, A. (1998). Lipopolysaccharide induces the antiapoptotic molecules, A1 and A20, in microvascular endothelial cells. *Blood*, **92**, 2759–2765.
15. Durkop, H., Hirsch, B., Hahn, C., Foss, H. D. & Stein, H. (2003). Differential expression and function of A20 and TRAF1 in Hodgkin lymphoma and anaplastic large cell lymphoma and their induction by CD30 stimulation. *J. Pathol.* **200**, 229–239.
16. Lee, E. G., Boone, D. L., Chai, S., Libby, S. L., Chien, M., Lodolce, J. P. & Ma, A. (2000). Failure to regulate TNF-induced NF-kappaB and cell death responses in A20-deficient mice. *Science*, **289**, 2350–2354.
17. Boone, D. L., Turer, E. E., Lee, E. G., Ahmad, R. C., Wheeler, M. T., Tsui, C. *et al.* (2004). The ubiquitin-modifying enzyme A20 is required for termination of Toll-like receptor responses. *Nat. Immunol.* **5**, 1052–1060.
18. Lin, R., Yang, L., Nakhaei, P., Sun, Q., Sharif-E. Askari, I. & Julkunen, J. (2006). Negative regulation of the retinoic acid-inducible gene I-induced antiviral state by the ubiquitin-editing protein A20. *J. Biol. Chem.* **281**, 2095–2103.
19. Wang, Y. Y., Li, L., Han, K. J., Zhai, Z. & Shu, H. B. (2004). A20 is a potent inhibitor of TLR3- and Sendai virus-induced activation of NF-kappaB and ISRE and IFN-beta promoter. *FEBS Lett.* **576**, 86–90.
20. Saitoh, T., Yamamoto, M., Miyagishi, M., Taira, K., Nakanishi, M., Fujita, T. *et al.* (2005). A20 is a negative regulator of IFN regulatory factor 3 signaling. *J. Immunol.* **174**, 1507–1512.
21. Hayden, M. S. & Ghosh, S. (2004). Signaling to NF-kappaB. *Genes Dev.* **18**, 2195–2224.
22. Heyninck, K. & Beyaert, R. (1999). The cytokine-inducible zinc finger protein A20 inhibits IL-1-induced NF-kappaB activation at the level of TRAF6. *FEBS Lett.* **442**, 147–150.
23. Heyninck, K., De Valck, D., Vanden Berghe, W., Van Criekinge, W., Contreras, R., Fiers, W. *et al.* (1999). The zinc finger protein A20 inhibits TNF-induced NF-kappaB-dependent gene expression by interfering with an RIP- or TRAF2-mediated transactivation signal and directly binds to a novel NF-kappaB-inhibiting protein ABIN. *J. Cell Biol.* **145**, 1471–1482.
24. Wertz, I. E., O'Rourke, K. M., Zhou, H., Eby, M., Aravind, L., Seshagiri, S. *et al.* (2004). De-ubiquitination and ubiquitin ligase domains of A20 down-regulate NF-kappaB signalling. *Nature*, **430**, 694–699.
25. Zhang, S. Q., Kovalenko, A., Cantarella, G. & Wallach, D. (2000). Recruitment of the IKK signalosome to the p55 TNF receptor: RIP and A20 bind to NEMO (IKKgamma) upon receptor stimulation. *Immunity*, **12**, 301–311.
26. Chen, Z. J. (2005). Ubiquitin signalling in the NF-kappaB pathway. *Nat. Cell Biol.* **7**, 758–765.
27. Deng, L., Wang, C., Spencer, E., Yang, L., Braun, A., You, J. *et al.* (2000). Activation of the IkappaB kinase complex by TRAF6 requires a dimeric ubiquitin-conjugating enzyme complex and a unique polyubiquitin chain. *Cell*, **103**, 351–361.
28. Wang, C., Deng, L., Hong, M., Akkaraju, G. R., Inoue, J. & Chen, Z. J. (2001). TAK1 is a ubiquitin-dependent kinase of MKK and IKK. *Nature*, **412**, 346–351.
29. Lamothe, B., Besse, A., Campos, A. D., Webster, W. K., Wu, H. & Darnay, B. G. (2007). Site-specific Lys-63-linked tumor necrosis factor receptor-associated factor 6 auto-ubiquitination is a critical determinant of I kappa B kinase activation. *J. Biol. Chem.* **282**, 4102–4112.
30. Ninomiya-Tsuji, J., Kishimoto, K., Hiyama, A., Inoue, J., Cao, Z. & Matsumoto, K. (1999). The kinase TAK1 can activate the NIK-I kappaB as well as the MAP kinase cascade in the IL-1 signalling pathway. *Nature*, **398**, 252–256.
31. Holtmann, H., Enninga, J., Kalble, S., Thiefes, A., Dorrie, A., Broemer, M. *et al.* (2001). The MAPK kinase kinase TAK1 plays a central role in coupling the interleukin-1 receptor to both transcriptional and RNA-targeted mechanisms of gene regulation. *J. Biol. Chem.* **276**, 3508–3516.
32. Irie, T., Muta, T. & Takeshige, K. (2000). TAK1 mediates an activation signal from toll-like receptor(s) to nuclear factor-kappaB in lipopolysaccharide-stimulated macrophages. *FEBS Lett.* **467**, 160–164.
33. Lee, J., Mira-Arbibe, L. & Ulevitch, R. J. (2000). TAK1 regulates multiple protein kinase cascades activated by bacterial lipopolysaccharide. *J. Leukocyte Biol.* **68**, 909–915.
34. Jiang, Z., Zamanian-Daryoush, M., Nie, H., Silva, A. M., Williams, B. R. & Li, X. (2003). Poly(I–C)-induced Toll-like receptor 3 (TLR3)-mediated activation of NFkappa B and MAP kinase is through an interleukin-1 receptor-associated kinase (IRAK)-independent pathway employing the signaling components TLR3–TRAF6–TAK1–TAB2–PKR. *J. Biol. Chem.* **278**, 16713–16719.

35. Mizukami, J., Takaesu, G., Akatsuka, H., Sakurai, H., Ninomiya-Tsuji, J., Matsumoto, K. & Sakurai, N. (2002). Receptor activator of NF-kappaB ligand (RANKL) activates TAK1 mitogen-activated protein kinase kinase kinase through a signaling complex containing RANK, TAB2, and TRAF6. *Mol. Cell Biol.* **22**, 992–1000.
36. Shibuya, H., Yamaguchi, K., Shirakabe, K., Tonegawa, A., Gotoh, Y., Ueno, N. *et al.* (1996). TAB1: an activator of the TAK1 MAPKKK in TGF-beta signal transduction. *Science*, **272**, 1179–1182.
37. Takaesu, G., Kishida, S., Hiyama, A., Yamaguchi, K., Shibuya, H., Irie, K. *et al.* (2000). TAB2, a novel adaptor protein, mediates activation of TAK1 MAPKKK by linking TAK1 to TRAF6 in the IL-1 signal transduction pathway. *Mol. Cell*, **5**, 649–658.
38. Ishitani, T., Takaesu, G., Ninomiya-Tsuji, J., Shibuya, H., Gaynor, R. B. & Matsumoto, K. (2003). Role of the TAB2-related protein TAB3 in IL-1 and TNF signaling. *EMBO J.* **22**, 6277–6288.
39. Cheung, P. C., Nebreda, A. R. & Cohen, P. (2004). TAB3, a new binding partner of the protein kinase TAK1. *Biochem. J.* **378**, 27–34.
40. Jin, G., Klika, A., Callahan, M., Faga, B., Danzig, J., Jiang, Z. *et al.* (2004). Identification of a human NF-{kappa}B-activating protein, TAB3. *Proc. Natl Acad. Sci. USA*, **101**, 2028–2033.
41. Besse, A., Lamothe, B., Campos, A. D., Webster, W. K., Maddineni, U., Lin, S. C. *et al.* (2007). TAK1-dependent signaling requires functional interaction with TAB2/TAB3. *J. Biol. Chem.* **282**, 3918–3928.
42. Kanayama, A., Seth, R. B., Sun, L., Ea, C. K., Hong, M., Shaito, A. *et al.* (2004). TAB2 and TAB3 activate the NF-kappaB pathway through binding to polyubiquitin chains. *Mol. Cell*, **15**, 535–548.
43. Heyninck, K. & Beyaert, R. (2005). A20 inhibits NF-kappaB activation by dual ubiquitin-editing functions. *Trends Biochem. Sci.* **30**, 1–4.
44. Evans, P. C., Ovaa, H., Hamon, M., Kilshaw, P. J., Hamm, S., Bauer, S. *et al.* (2004). Zinc-finger protein A20, a regulator of inflammation and cell survival, has de-ubiquitinating activity. *Biochem. J.* **378**, 727–734.
45. Klinkenberg, M., Van Huffel, S., Heyninck, K. & Beyaert, R. (2001). Functional redundancy of the zinc fingers of A20 for inhibition of NF-kappaB activation and protein–protein interactions. *FEBS Lett.* **498**, 93–97.
46. Amerik, A. Y. & Hochstrasser, M. (2004). Mechanism and function of deubiquitinating enzymes. *Biochim. Biophys. Acta*, **1695**, 189–207.
47. Nijman, S. M., Luna-Vargas, M. P., Velds, A., Brummelkamp, T. R., Dirac, A. M., Sixma, T. K. & Bernards, R. (2005). A genomic and functional inventory of deubiquitinating enzymes. *Cell*, **123**, 773–786.
48. Makarova, K. S., Aravind, L. & Koonin, E. V. (2000). A novel superfamily of predicted cysteine proteases from eukaryotes, viruses and *Chlamydia pneumoniae*. *Trends Biochem. Sci.* **25**, 50–52.
49. Yeates, T. O. (1997). Detecting and overcoming crystal twinning. *Methods Enzymol.* **276**, 344–358.
50. Lee, S., Sawaya, M. R. & Eisenberg, D. (2003). Structure of superoxide dismutase from *Pyrobaculum aerophilum* presents a challenging case in molecular replacement with multiple molecules, pseudo-symmetry and twinning. *Acta Crystallogr. Sect. D*, **59**, 2191–2199.
51. Evans, P. C., Taylor, E. R., Coadwell, J., Heyninck, K., Beyaert, R. & Kilshaw, P. J. (2001). Isolation and characterization of two novel A20-like proteins. *Biochem. J.* **357**, 617–623.
52. Johnston, S. C., Riddle, S. M., Cohen, R. E. & Hill, C. P. (1999). Structural basis for the specificity of ubiquitin C-terminal hydrolases. *EMBO J.* **18**, 3877–3887.
53. Misaghi, S., Galardy, P. J., Meester, W. J., Ovaa, H., Ploegh, H. L. & Gaudet, R. (2005). Structure of the ubiquitin hydrolase UCH-L3 complexed with a suicide substrate. *J. Biol. Chem.* **280**, 1512–1520.
54. Hu, M., Li, P., Li, M., Li, W., Yao, T., Wu, J. W. *et al.* (2002). Crystal structure of a UBP-family deubiquitinating enzyme in isolation and in complex with ubiquitin aldehyde. *Cell*, **111**, 1041–1054.
55. Hu, M., Li, P., Song, L., Jeffrey, P. D., Chenova, T. A., Wilkinson, K. D. *et al.* (2005). Structure and mechanisms of the proteasome-associated deubiquitinating enzyme USP14. *EMBO J.* **24**, 3747–3756.
56. Renatus, M., Parrado, S. G., D'Arcy, A., Eidhoff, U., Gerhartz, B., Hassiepen, U. *et al.* (2006). Structural basis of ubiquitin recognition by the deubiquitinating protease USP2. *Structure*, **14**, 1293–1302.
57. Nanao, M. H., Tcherniuk, S. O., Chroboczek, J., Dideberg, O., Dessen, A. & Balakirev, M. Y. (2004). Crystal structure of human otubain 2. *EMBO Rep.* **5**, 783–788.
58. King, R. C. & Storto, P. D. (1988). The role of the otu gene in *Drosophila* oogenesis. *Bioessays*, **8**, 18–24.
59. Rawlings, N. D., O'Brien, E. & Barrett, A. J. (2002). MEROPS: the protease database. *Nucleic Acids Res.* **30**, 343–346.
60. Hershko, A. & Rose, I. A. (1987). Ubiquitin-aldehyde: a general inhibitor of ubiquitin-recycling processes. *Proc. Natl Acad. Sci. USA*, **84**, 1829–1833.
61. Borodovsky, A., Ovaa, H., Kolli, N., Gan-Erdene, T., Wilkinson, K. D., Ploegh, H. L. & Kessler, B. M. (2002). Chemistry-based functional proteomics reveals novel members of the deubiquitinating enzyme family. *Chem. Biol.* **9**, 1149–1159.
62. Pickart, C. M. & Rose, I. A. (1986). Mechanism of ubiquitin carboxyl-terminal hydrolase. Borohydride and hydroxylamine inactivate in the presence of ubiquitin. *J. Biol. Chem.* **261**, 10210–10217.
63. Dang, L. C., Melandri, F. D. & Stein, R. L. (1998). Kinetic and mechanistic studies on the hydrolysis of ubiquitin C-terminal 7-amido-4-methylcoumarin by deubiquitinating enzymes. *Biochemistry*, **37**, 1868–1879.
64. Hochrainer, K. & Lipp, J. (2007). Ubiquitylation within signaling pathways in- and outside of inflammation. *Thromb. Haemost.* **97**, 370–377.
65. Komander, D. & Barford, D. (2008). Structure of the A20 OTU domain and mechanistic insights into deubiquitination. *Biochem J.* **409**, 77–85.
66. Padilla, J. E. & Yeates, T. O. (2003). A statistic for local intensity differences: robustness to anisotropy and pseudo-centering and utility for detecting twinning. *Acta Crystallogr. Sect. D*, **59**, 1124–1130.